Optimal Feeding for Tower-Type Reactors

Chun-Chong Fu, Shih-Yuan Lu, Wen-Teng Wu
Dept. of Chemical Engineering, National Tsing-Hua University, Hsin-Chu, 30043, Taiwan

DOI 10.1002/aic.10346
Published online in Wiley InterScience (www.interscience.wiley.com).

In tower-type reactors, poor mixing is a major concern in fermentation processes. As an attempt to improve the mixing efficiency, an algorithm based on the analytic solution of the modified network-of-zones model and application of the singular value decomposition technique is proposed to determine the optimal feeding locations and corresponding amounts of feed in airlift reactors, bubble column reactors, and airlift reactors with wire-mesh draft tube. The optimal feeding locations and corresponding amounts of feed predicted by the algorithm are in good agreement with the experimental results. The proposed algorithm is proved to be an effective method for optimizing the feeding operation to improve the mixing efficiency for the three tower-type reactors. © 2005 American Institute of Chemical Engineers *AIChE J,* 51: 713–724, 2005
Keywords: network-of-zones model, optimal feeding, mixing efficiency, airlift reactor, bubble column

Introduction

Bubble column[1] and airlift reactors[2] are tower-type reactors widely used in biotechnological processes. Tower-type reactors make use of the kinetic energy of gas bubbles to achieve mixing and aeration. The common feature of this type of reactor is the gas supply in the bottom of the reactor. The gas flow creates a density difference in the liquid region, which drives liquid circulation of a particular pattern. Also, this liquid movement helps to promote the necessary mixing and mass transfer.

Lack of moving parts, lower power consumption, and less shear stress are the main advantages of these reactors over the stirred-tank reactors for use in bioprocesses. They are suitable for systems involving shear-sensitive microorganisms. However, compared to mechanical agitation, poorer mass transfer and mixing performance are the major disadvantages in application of these reactors.[3]

A great deal of effort has been devoted to improve the mixing efficiency of these reactors, mostly in the modification of the reactor design. Airlift reactor with wire-mesh draft tube, hereafter called *net column reactor* for convenience, is an example of the modified tower-type reactors possessing an improved mixing performance. The superiority of net column reactors has been demonstrated in many microorganism fermentation systems, including production of Baker's yeast, glutamic acid, thuringiensin, chitosan, red pigment from *Monascus*, and bacterial cellulose.[4,5] A net column reactor is a good design in balancing flow distribution in the axial and radial directions, when compared with bubble column and airlift reactors under the same aeration rate. The above statement has been theoretically and experimentally confirmed by Fu et al.[6] in terms of two indicators, the slowest mode eigenvalue of the modified network-of-zones model, and mixing time for pulse feeding.

In this article, we take a different approach to improve the mixing efficiency of tower-type reactors. We design an optimal feeding strategy, in terms of feeding locations and their associated amounts of feed, to achieve faster mixing in tower-type reactors, by exploring the analytical solution of the modified network-of-zones model and by using the singular value decomposition (SVD) technique.[7] Experiments are conducted to verify the proposed scheme with the heat tracer response method. The model prediction for the optimal feeding arrangement agrees well with the experimental results.

Experimental

In this section, an algorithm, based on the analytic solution of the modified network-of-zones model and the application of

Correspondence concerning this article should be addressed to W.-T. Wu at wtwu@mail.ncku.edu.tw.

SVD, is devised to determine the optimal initial condition vector, which contains the information for feeding locations and the associated amounts of feed, for any preset targeted mixing time and concentration tolerance. The problem statement may be more clearly described as follows. For a given tower-type reactor, when fed with a certain amount of feed, the concentration of the feed species in the reactor goes through a dynamics before finally reaching a new steady state of uniform concentration. Mathematically speaking, the time needed to reach the new steady state—in theory—is infinitely long. Therefore, a concentration tolerance is used to judge whether the concentration field is close enough to the new steady-state concentration, and the mixing time is defined as the minimal elapsed time needed to bring the concentration field within the tolerance range of the new steady-state concentration. One major design concern is the number of feedports used. Apparently, the more feedports used, the shorter the required mixing time. In practical applications, however, the number of feedports should be kept minimal to avoid operation complication. Now, consider the following problem. One feeds a certain amount of feed into a tower-type reactor and demands that the steady state within a preset tolerance be achieved in a targeted mixing time. The questions are: What is the minimum number of feedports required? How should one arrange the feedport location and the associated amount of feed to accomplish the mission?

We are basically dealing with an inverse problem, given the target and requested feasible initial condition. The basic logic flow of the algorithm development is summarized as follows. First, the modified network-of-zones model is used to simulate the flow and mixing behavior of the three tower-type reactors. The model divides the fluid domain of the reactor into n well-stirred parcels and formulates the governing equations for concentration field, $\underline{C}(t)$, through mass balance of the feed species. The end result is a set of linear ordinary differential equations for the n parcel concentrations, whose solution vector may be expressed as the initial condition vector (initial concentrations for the n parcels representing the feeds, $\underline{C}_0$) premultiplied by a matrix, $\mathbf{E}(t)$, which contains the eigenvalues and corresponding eigenvectors of the coefficient matrix of the linear system. The inverse problem can then be tackled by examining the singularity of $\mathbf{E}(t)$ with the SVD technique given a targeted mixing time (t_m) and concentration tolerance (ε). The measure of singularity is the rank of the matrix, k, which gives the degrees of freedom of the system at the desired state. Consequently, there are $n - k$ initial concentrations to be specified at will and k initial concentrations left to be solved. Because one wants a minimum number of feedports, the $n - k$ initial concentrations are to be set as zeros for no feeding at these locations. Thus, the minimum number of feedports is k and the associated amounts of feed can be uniquely determined from solving the remaining $k \times k$ linear equation set. Because there are many different ways of picking out k feedports from n locations, one has to run through all possible combinations and obtain solutions for all of them. Some of the solutions may contain negative amounts of feed, which are not feasible and should be discarded. Among the remaining feasible solutions for the initial condition vector, one can now determine the corresponding mixing times by solving for their concentration dynamics and comparing with the preset concentration tolerance range. Finally, one can obtain the optimal combination of feedport locations and associated amounts of feed, which give the shortest mixing time.

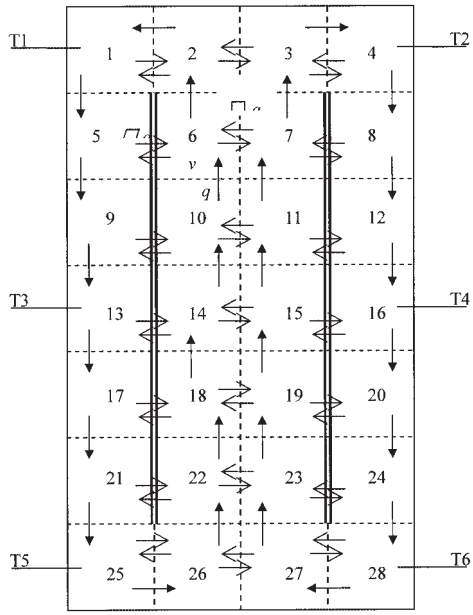

Figure 1. Network-of-zones representation of the reactor.

Modified network-of-zones model for tower-type reactors

The modified network-of-zones model is used to simulate the nonreactive flow and liquid-phase mixing behavior in the tower-type reactors that are represented as connected ideal well-mixed parcels, as shown in Figure 1. Neighboring zones are connected to form a parcel network. The bold arrows indicate the main circular convective flow and the thin arrows denote the radial interactions of neighboring parcels. The double lines denote the draft tube options: (1) a solid wall draft tube for the airlift reactor, (2) no draft tube for the bubble column, and (3) a wire-mesh draft tube for the net column reactor. Based on the principle of mass balance for feed species in each parcel, a set of linear ordinary differential equations (ODEs) is formulated to simulate the mixing behavior of these reactors. For example, the linear ODEs based on the mole balance for parcels 1, 2, and 3 are given as

$$
\begin{aligned}
v\frac{dC_1}{dt} &= -(1+\beta)qC_1 + (1+\beta)qC_2 \\
v\frac{dC_2}{dt} &= -(1+\alpha+\beta)qC_2 + \alpha qC_3 + qC_6 + \beta qC_1 \\
v\frac{dC_3}{dt} &= -(1+\alpha+\beta)qC_3 + \alpha qC_2 + qC_7 + \beta qC_4 \qquad (1)
\end{aligned}
$$

where C_i is the concentration at the ith parcel, α is the dimensionless interaction strength between neighboring uprising streams, β is the dimensionless interaction strength between neighboring uprising and downcoming streams, v is the parcel volume, and q is the volumetric flow rate of the

main convective flow. The term β is the key parameter that differentiates the type of tower reactor in the modified network-of-zones model. For example, when β is set as zero, it means that there is no fluid interaction between the riser and downcomer, and an airlift reactor is modeled. For bubble column reactors, there are intensive interactions between the neighboring uprising and downcoming streams such that a large value should be assigned for β. With respect to net column reactors, the relevant interactions are moderate and an intermediate value is appropriate. For more detailed description of the modified network-of-zones model, the reader should consult our previous publication as listed in Fu et al.[6]

The governing equations for all parcels of the system can be expressed in the matrix form as follows

$$\begin{bmatrix} C_1' \\ C_2' \\ C_3' \\ \vdots \\ C_n' \end{bmatrix} = \begin{bmatrix} -(1+\beta)\omega & (1+\beta)\omega & 0 & \cdots & 0 \\ \beta\omega & -(1+\alpha+\beta)\omega & \alpha\omega & \cdots & 0 \\ 0 & \alpha\omega & -(1+\alpha+\beta)\omega & \cdots & 0 \\ \vdots & \vdots & \vdots & \cdots & \vdots \\ 0 & 0 & 0 & \cdots & -(1+\beta)\omega \end{bmatrix} \begin{bmatrix} C_1 \\ C_2 \\ C_3 \\ \vdots \\ C_n \end{bmatrix} \tag{2}$$

where ω is the reciprocal of the time needed to fill an empty parcel of volume v with the volumetric flow rate q, and the subscript n denotes the number of parcels used to model the flow system. The superscript prime denotes the derivative with respect to time. If $[C_1' \ C_2' \ C_3' \ \cdots \ C_n']^T$ is denoted by $\underline{C}'$, $[C_1 \ C_2 \ C_3 \ \cdots \ C_n]^T$ by $\underline{C}$, and the coefficient by $\mathbf{A}$, then Eq. 2 can be simply described as

$$\underline{C}' = \mathbf{A}\underline{C} \tag{3}$$

By using a similar transformation,[8] the analytical solution of Eq. 3 can be derived. The general solution of $\underline{C}$ can be expressed as

$$\underline{C} = \mathbf{P}e^{\mathbf{\Lambda}t}\mathbf{P}^{-1}\underline{C}_0 \tag{4}$$

where $\mathbf{\Lambda}$ is a diagonal matrix composed of eigenvalues of $\mathbf{A}$, $\mathbf{P}$ denotes the matrix constructed from the corresponding eigenvectors, the superscript -1 denotes the inverse of the matrix, $\underline{C}_0$ is the initial condition vector, and t is time.

Application of singular value decomposition

Because $\underline{C}(t)$ is a function of time and initial condition vector, the implication is that a desired optimal initial condition vector $\underline{C}_0$ can be found with the targeted $\underline{C}(t)$ and t specified. This is an inverse problem and can be tackled by examining the singularity of the system with the SVD technique for the present problem. Let $\mathbf{E}(t) = \mathbf{P}e^{\mathbf{\Lambda}t}\mathbf{P}^{-1}$. Then Eq. 4 is written as

$$\underline{C}(t) = \mathbf{E}(t)\underline{C}_0 \tag{5}$$

If $\underline{C}_0$ is not a zero vector, a steady state can be reached at infinitely long time

$$\underline{C}^* = \mathbf{E}(\infty)\underline{C}_0 \qquad \underline{C}_0 \neq \underline{0} \qquad t \to \infty \tag{6}$$

The new steady state, $\underline{C}^*$, in Eq. 6 signifies the uniformity in concentration for all parcels, so that all elements of $\underline{C}^*$ are the same. At a sufficiently long time, denoted by t_m, we have

$$\underline{C}(t_m) = \mathbf{E}(t_m)\underline{C}_0 \tag{7}$$

The constraint for t_m is given as follows

$$\frac{|c_i(t_m) - c^*|}{c^*} \leq \varepsilon \tag{8}$$

where $|\ \ |$ denotes the absolute value of a scalar. The quantity t_m is defined as the mixing time, which is the minimal time at which the normalized concentration difference of every parcel becomes less than a preset tolerance value ε, as shown in Eq. 8. Here, $c_i(t_m)$ and c^* denote the components of $\underline{C}(t_m)$ and $\underline{C}^*$ of parcel i, respectively.

By using $\mathbf{E}(t_m)$ to approximate $\mathbf{E}(\infty)$,$\underline{C}_0$ is obtained by taking the inverse of $\mathbf{E}(t_m)$, as follows

$$\underline{C}_0 \cong \mathbf{E}(t_m)^{-1}\underline{C}^* \tag{9}$$

However, the inverse of matrix $\mathbf{E}(t_m)$ does not always exist because the matrix is possibly singular. To obtain $\underline{C}_0$, the singularity of $\mathbf{E}(t_m)$ has to be examined. The SVD technique is used to determine the singularity of the matrix.[7] According to the SVD procedure, the matrix $\mathbf{E}(t_m)$ is decomposed into $\mathbf{U}$, $\mathbf{V}$, and $\mathbf{\Sigma}$. $\mathbf{U}$ and $\mathbf{V}$ are the left and right singular matrices. Both of the matrices are unitary matrices. $\mathbf{\Sigma}$ is a diagonal matrix, composed of nonnegative singular values. The above statement can be described as

$$\mathbf{E}(t_m) = \mathbf{U}\mathbf{\Sigma}\mathbf{V}^T \tag{10}$$

By combining Eqs. 7, 8, and 10, we obtain the following equation in the matrix form

$$\|(\mathbf{U}\mathbf{\Sigma}\mathbf{V}^T)\underline{C}_0 - \underline{C}^*\|_2 \leq \|\varepsilon\underline{C}^*\|_2 \tag{11}$$

$\|\ \ \|_2$ means the 2-norm of a vector. If $\underline{C}^*$ is the initial condition vector of the reactor, the steady state is still $\underline{C}^*$. Thus, $\underline{C}^*$ can be written as

$$\underline{C}^* = \mathbf{E}(t_m)\underline{C}^* = (\mathbf{U}\mathbf{\Sigma}\mathbf{V}^T)\underline{C}^*$$

Then, Eq. 11 can be rewritten as

$$\|(\mathbf{U}\mathbf{\Sigma}\mathbf{V}^T)\underline{C}_0 - (\mathbf{U}\mathbf{\Sigma}\mathbf{V}^T)\underline{C}^*\|_2 \le \|\varepsilon\underline{C}^*\|_2 \tag{12}$$

After premultiplying the corresponding matrix inequality by $\mathbf{U}^{-1}$, Eq.12 then becomes

$$\|\mathbf{\Sigma}\mathbf{V}^T\underline{C}_0 - \mathbf{\Sigma}\mathbf{V}^T\underline{C}^*\|_2 \le \|\varepsilon\mathbf{U}^{-1}\underline{C}^*\|_2 \tag{13}$$

Let

$$\underline{Y} = \mathbf{V}^T(\underline{C}_0 - \underline{C}^*) \tag{14}$$

then we obtain

$$\|\mathbf{\Sigma}\underline{Y}\|_2 \le \|\varepsilon\mathbf{U}^{-1}\underline{C}^*\|_2 \tag{15}$$

Expanding Eq. 15, based on the definition of 2-norm, gives

$$\sqrt{(\mathbf{\Sigma}\underline{Y})^T(\mathbf{\Sigma}\underline{Y})} \le \sqrt{(\varepsilon\mathbf{U}^{-1}\underline{C}^*)^T(\varepsilon\mathbf{U}^{-1}\underline{C}^*)} \tag{16a}$$

or

$$\sqrt{(\sigma_1 y_1)^2 + (\sigma_2 y_2)^2 + \cdots + (\sigma_n y_n)^2} \le \sqrt{n(\varepsilon c^*)^2} \tag{16b}$$

where σ_i represents the singular values, which are the diagonal components of $\mathbf{\Sigma}$, and y_j are the components of $\underline{Y}$. According to the definition of inner product of two vectors, y_j can be written as follows

$$y_j = \mathbf{V}_j^T(\underline{C}_0 - \underline{C}^*) = \|\mathbf{V}_j^T\|_2\|\underline{C}_0 - \underline{C}^*\|_2\cos\,\theta_j = 1 \times \|\underline{C}_0 - \underline{C}^*\|_2\cos\,\theta_j \tag{17}$$

where $\boldsymbol{V}_j^T$ is the jth row vector of the matrix $\mathbf{V}^T$. The value of $\|\boldsymbol{V}_j^T\|_2$ is equal to one, because $\mathbf{V}$ is an orthonormal matrix. Because of Eq. 17, Eq. 16b can be expressed as

$$\sqrt{(\sigma_1 y_1)^2 + (\sigma_2 y_2)^2 + \cdots + (\sigma_n y_n)^2} = \sqrt{(\sigma_1^2\cos^2\theta_1 + \sigma_2^2\cos^2\theta_2 + \cdots + \sigma_n^2\cos^2\theta_n)\|\underline{C}_0 - \underline{C}^*\|_2^2} \le \sqrt{n(\varepsilon c^*)^2} \tag{18}$$

The initial concentration vector, $\underline{C}_0$, has two extreme cases. One is that the feed is equally distributed to each parcel so that $\underline{C}_0 = [c^*\ c^*\ c^*\ \cdots\ c^*]_{n\times 1}^T$. The other case is that the feed is put in one single parcel. Let the feed be in parcel 1, then $\underline{C}_0 = [nc^*\ 0\ 0\ \cdots\ 0]_{n\times 1}^T$. Therefore, $\underline{C}_0 - \underline{C}^*$ is between $[0\ 0\ 0\ \cdots\ 0]_{n\times 1}^T$ and $[(n-1)c^*\ -c^*\ -c^*\ \cdots\ -c^*]_{n\times 1}^T$. With this, one concludes that $0 \le \|\underline{C}_0 - \underline{C}^*\|_2 \le \sqrt{n(n-1)}c^*$. Because $0 \le \cos^2\theta_j \le 1$, the term $(\sigma_1^2\cos^2\theta_1 + \sigma_2^2\cos^2\theta_2 + \cdots + \sigma_n^2\cos^2\theta_n)\|\underline{C}_0 - \underline{C}^*\|_2^2$ is restricted as follows

$$0 \le (\sigma_1^2\cos^2\theta_1 + \sigma_2^2\cos^2\theta_2 + \cdots + \sigma_n^2\cos^2\theta_n)\|\underline{C}_0 - \underline{C}^*\|_2^2 \le (\sigma_1^2 + \sigma_2^2 + \cdots + \sigma_n^2)n(n-1)(c^*)^2 \tag{19}$$

When the system reaches the state at $t = t_m$, Eq. 18 can be given as

$$(\sigma_1^2\cos^2\theta_1 + \sigma_2^2\cos^2\theta_2 + \cdots + \sigma_n^2\cos^2\theta_n)\|\underline{C}_0 - \underline{C}^*\|^2 \cong n(\varepsilon c^*)^2 \tag{20}$$

Consequently, Eq. 19 can be rewritten as the following equation by using Eq. 20

$$0 \le n(\varepsilon c^*)^2 \le (\sigma_1^2 + \sigma_2^2 + \cdots + \sigma_k^2 + \sigma_{k+1}^2 + \cdots + \sigma_n^2)n(n-1)(c^*)^2$$

or

$$0 \le \frac{\varepsilon^2}{n-1} \le (\sigma_1^2 + \sigma_2^2 + \cdots + \sigma_k^2 + \sigma_{k+1}^2 + \cdots + \sigma_n^2) \tag{21}$$

Because $\sigma_1 \ge \sigma_2 \ge \sigma_3 \ge \cdots \ge \sigma_n$, a suitable k can be chosen to satisfy the following equation

$$(\sigma_{k+1}^2 + \sigma_{k+2}^2 + \cdots + \sigma_n^2) \le \frac{\varepsilon^2}{n-1} < (\sigma_k^2 + \sigma_{k+1}^2 + \cdots + \sigma_n^2) \tag{22}$$

Let $\mathbf{\Sigma}_k$ be an $n\times n$ diagonal matrix with k singular values of $\mathbf{\Sigma}$, but zeros from σ_{k+1} to σ_n, as shown below

$$\mathbf{\Sigma}_k = \begin{bmatrix} \sigma_1 & 0 & \cdots & 0 & 0 & \cdots & 0 \\ 0 & \sigma_2 & \cdots & 0 & 0 & \cdots & 0 \\ \cdots & \cdots & \cdots & \cdots & \cdots & \cdots & \cdots \\ 0 & 0 & \cdots & \sigma_k & 0 & \cdots & 0 \\ 0 & 0 & \cdots & 0 & 0 & \cdots & 0 \\ \cdots & \cdots & \cdots & \cdots & \cdots & \cdots & \cdots \\ 0 & 0 & \cdots & 0 & 0 & \cdots & 0 \end{bmatrix}$$

Similarly, $\mathbf{\Sigma}_{k-1}$ is given as

$$\mathbf{\Sigma}_{k-1} = \begin{bmatrix} \sigma_0 & 0 & \cdots & 0 & 0 & \cdots & 0 \\ 0 & \sigma_2 & \cdots & 0 & 0 & \cdots & 0 \\ \cdots & \cdots & \cdots & \cdots & \cdots & \cdots & \cdots \\ 0 & 0 & \cdots & \sigma_{k-1} & 0 & \cdots & 0 \\ 0 & 0 & \cdots & 0 & 0 & \cdots & 0 \\ \cdots & \cdots & \cdots & \cdots & \cdots & \cdots & \cdots \\ 0 & 0 & \cdots & 0 & 0 & \cdots & 0 \end{bmatrix}$$

The ranks of $\mathbf{\Sigma}_k$ and $\mathbf{\Sigma}_{k-1}$ equal k and $k-1$, respectively, according to the Key Corollary 8.20 of *Applied Linear Algebra*.[7] The rank is the number of nonzero singular values of the matrix. Equation 22 can now be written as

Table 1. Model Parameters for Airlift, Bubble Column, and Net Column Reactors

Reactor Type	n (Parcel Number)	Parameter α	β	ω
Airlift reactor	28	5	0	1.85*
Bubble column reactor	28	5	5	1.47*
Net column reactor	28	5	0.9*	1.42*

*Values obtained from fitting model with experimental data at gas flow rate of 10 LPM.

$$\|\mathbf{\Sigma} - \mathbf{\Sigma}_k\|_2 \leq \sqrt{\frac{\varepsilon^2}{n-1}} < \|\mathbf{\Sigma} - \mathbf{\Sigma}_{k-1}\|_2 \tag{23}$$

According to Theorem 8.21 of *Applied Linear Algebra*,[7] the rank of $\mathbf{\Sigma}$ can be shown to equal k, which implies that the rank of $\mathbf{E}(t_m)$ is also equal to k.

Because the magnitude of ε affects the truncated length of the sequence number of the singular values, the subscript k is certainly a function of ε. According to Eqs. 2, 10, and 22, the rank of $\mathbf{E}(t_m)$ depends on t, ω, α, and β, when ε and t_m are given.

Optimization of initial conditions

Because $\underline{C}_0$ is composed of n components, the determined rank k of the matrix $\mathbf{E}(t_m)$ implies the situation of underdetermination as well as the existence of infinite solutions. One way to obtain unique solutions is to zero $n - k$ components of $\underline{C}_0$ as no feeding at these corresponding locations. The resulting solutions, which indicate the feeding locations and amounts of feed in the initial state, are expected to meet the criterion of Eq. 8 in t_m. With a given rank of $\mathbf{E}(t_m)$, the optimal feasible solution for $\underline{C}_0$ may be obtained by the following three steps.

(1) Zero $n - k$ components of $\underline{C}_0$ to represent the situation of a k feedport operation. One simple example is as follows

$$\mathbf{E}(t_m)\underline{C}_0 = \underline{C}^*$$
$$c_{0j} = 0 \qquad \text{for} \qquad k+1 \leq j \leq n \tag{24}$$

where c_{0j} is the jth component of $\underline{C}_0$. Here, the first k locations are assigned feedports, whereas the latter $n - k$ locations allow no feeding. A unique solution for $\underline{C}_0$ can be obtained by solving Eq. 24, and the nonzero components of the resulting $\underline{C}_0$ are the amounts of feed for the k feedports.

(2) Obtain unique solutions for $\underline{C}_0$ for all $C_k^n = n!/[(n-k)! \times k!]$ possible combinations of feedport locations. Note the example shown in Eq. 24 is just one of the C_k^n possible combinations.

(3) Discard those solutions for $\underline{C}_0$ that contain nonrealistic negative amounts of feed. The remaining initial condition vectors are the feasible ones. With the initial condition vectors obtained, one can then use them in Eq. 4 to solve for the corresponding concentration dynamics and obtain the resulting mixing time under the condition of a preset concentration tolerance. The one giving the shortest mixing time is the optimal initial condition vector and represents the optimal feeding operation.

Experiments

To verify the validity of the above theoretical development, experiments based on the heat tracer response method are conducted in a transparent acrylic tower reactor whose dimension is 13 cm in diameter and 100 cm in height. The reactor is equipped with a circular sparger, 8.5 cm in diameter, having 36 holes of 1 mm diameter, and is mounted concentrically at the bottom of the reactor. The draft tubes used for the airlift reactor and the net column reactor are 8.5 cm in diameter and 75 cm in height. The reactor is filled with water to the level of 91 cm from the bottom.

The temperature response of the liquid inside the reactor is measured with six K-type thermocouples at the positions of T1 through T6. The six thermocouples are located at heights of 5, 46, and 87 cm from the bottom of the reactor and the tip of the thermocouples are kept 1.6 cm into the reactor. T1 to T6 are located in parcels 1, 4, 13, 16, 25, and 28, respectively, as shown in Figure 1. Three of the thermocouples are located on one side of the reactor and the remaining three on the opposite side. The location of the thermocouples enables us to investigate the temperature responses at the top, middle, and bottom regions of the reactor and to check the dynamics when the heat tracer is added at the designate locations.

Parameter estimation

For parameter estimation, the least-squares method is used to minimize the objective deviation function, which is the sum of the squared difference between the experimental and simulated time series data. The flow domain within the reactor is divided into three regions: top (parcels 1–4), middle (parcels 5–24), and bottom (parcels 25–28). The concentration dynamics at the parcels where the thermocouples are located are simulated using Eq. 4 and the experimental time series data are captured from the thermocouples. There are four model parameters n, α, β, and ω to be determined or fitted.

(1) n: The number of parcels used to represent the flow domain of the reactor. The use of 28 compartments is adopted according to the circulation cell model proposed by Joshi and Sharma in 1979.[9] Its value is estimated as four times the ratio of the fluid height to reactor diameter. A setting of 28 for n is found appropriate and satisfactory. Because we need at least four parcels in the horizontal plane to account for the two inner uprising streams and the two outer downcoming streams, we are left with the choice of 7 parcels for the axial direction.

(2) β: The interaction strength between the neighboring uprising and downcoming streams. Its value is set as 0 when there is no interaction between the neighboring uprising and downcoming streams as in the case of the airlift reactor equipped with a solid wall draft tube. As β moves gradually away from 0, the interaction between the neighboring uprising and downcoming streams becomes increasingly stronger. For the present three tower-type reactors, the fundamental difference between them is the draft tube usage. There is no draft tube for the bubble column reactor, whereas a draft tube is present in the airlift and net column reactors. The flow domain may be divided into three regions: top, middle, and bottom. The top region is the region above the draft tube, that is, parcels 1 to 4 in Figure 1, whereas the bottom region is the region below the draft tube, that is, parcels 25 to 28 in Figure 1. The rest belongs to the middle region. Because of the intensive

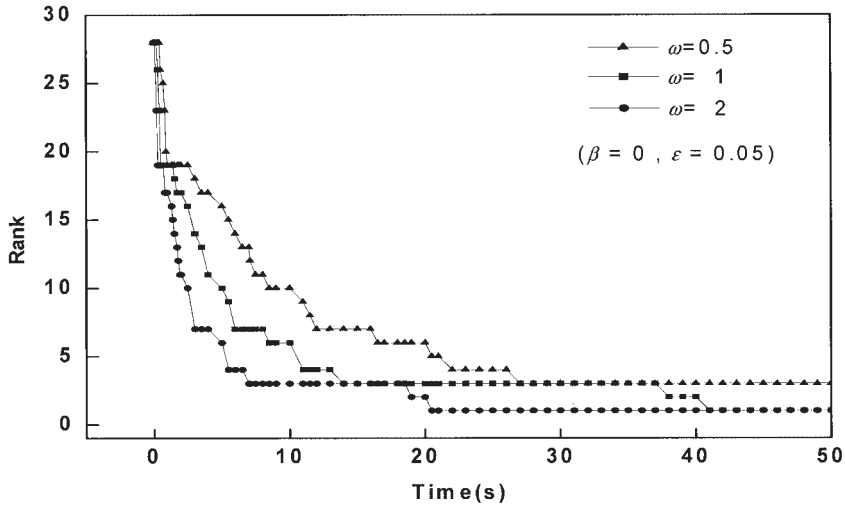

(a)

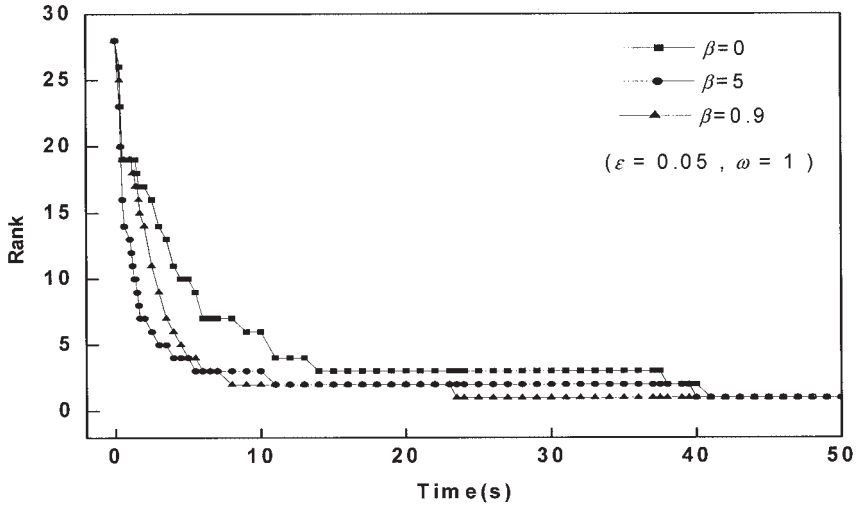

(b)

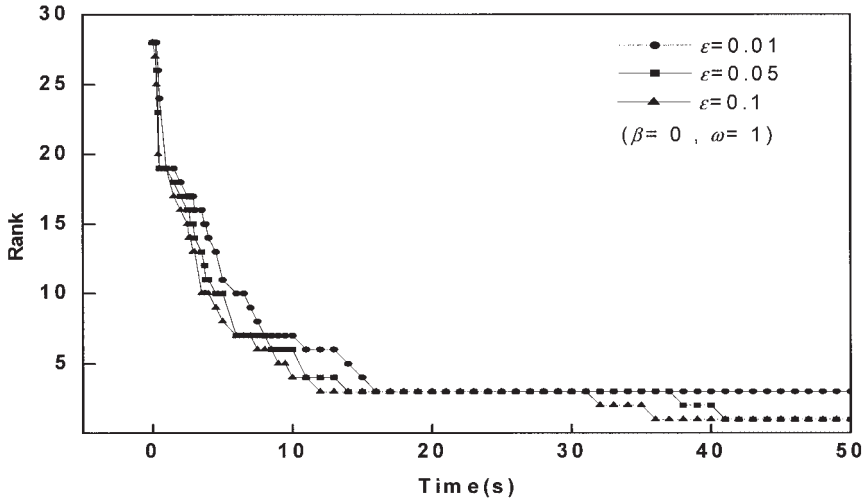

(c)

Figure 2. Rank of E(*t*) vs. desired mixing time with (a) ω, (b) β, and (c) ε as the varying parameters.

Table 2. Predicted Mixing Times for Single-Port Feedings at Several Feeding Locations for Airlift Reactors ($\alpha = 5$, $\beta = 0$, $\omega = 1$), Bubble Column Reactors ($\alpha = 5$, $\beta = 5$, $\omega = 1$), and Net Column Reactors ($\alpha = 5$, $\beta = 0.9$, $\omega = 1$); $\varepsilon = \pm 5\%$

Parcel Number (Feeding Location)	Amount of Feed	Predicted Mixing Time (s)		
		Airlift Reactor	Bubble Column Reactor	Net Column Reactor
1	28	29.4	30.8	18.2
2	28	29.5	31.0	18.3
5	28	31.0	28.7	15.8
6	28	29.9	29.3	17.9
9	28	31.0	23.2	10.5
10	28	30.6	24.8	16.1
13	28	31.0	9.9	11.6

mixing observed from experiments in the top and bottom regions, the β values in these two regions are always set at 5 regardless of the concerned reactor type. Note that the mixing performance becomes irrelevant to β when β is set large enough and 5 is a suitable value to represent this well-mixed condition. With respect to the middle region, the setting of β needs further discussion. For airlift reactors, the draft tube is with a solid wall resulting in no interaction between the neighboring uprising and downcoming streams such that β *should* be set zero. For bubble column reactors, no draft tube is present and the interaction between the neighboring uprising and downcoming streams can be considered intensive enough to justify a setting of 5 for β.[6] As for net column reactors, the draft tube is with a net wall, allowing partial stream interactions. One expects the value of β to be >0 but <5. We determine this value for net column reactors by fitting the model prediction with experimental measurements. This parameter has been shown in Fu et al.[6] to play a decisive role of determining the mixing performance of the three tower-type reactors.

(3) ω: Defined as the reciprocal of the time needed to fill an empty parcel, of a volume v, at a volumetric flow rate q. A larger ω signifies a faster main convective flow and normally speeds up the mixing process. We determine this parameter by fitting model predictions with experimental measurements for all three types of reactors.

(4) α: The interaction strength between the neighboring uprising streams. Larger values of α lead to smaller concentration differences between the neighboring uprising streams. From experimental observations, intensive interactions always exist between neighboring uprising streams for all three types of reactors, and thus a setting of 5 for α is used regardless of reactor type. Note that we observe from model outputs that mixing performance becomes insensitive to α when α is >0.3. Therefore, a setting of 5 for α is appropriate.[6]

With the above discussion, we need to fit for ω for airlift and bubble column reactors, whereas a 2-D fitting in the ω and β domains is necessary for net column reactors. The results for parameter setting and fitting under the aeration condition of 10 LPM are tabulated in Table 1. Note that a β value of 0.9, between 0 and 5 as expected, is obtained for net column reactors.

Results and Discussion

Rank of E(t) as a function of β, ω, and ε

As discussed in previous sections, the rank of $\mathbf{E}(t)$ carries important information for the mixing performance of the system. It can be interpreted as the minimum number of feedports necessary to achieve a mixed state within the preset concentration tolerance range in a targeted mixing time of t. One can expect, for shorter t, that more feedports are needed, whereas for longer t, fewer feedports are sufficient. Consequently, the rank of $\mathbf{E}(t)$, depending on α, β, ω, and ε, reduces digitally from the full rank n (28 here) to 1 with increasing targeted mixing time. Among the four parameters, α is set at 5 as a constant, whereas the other three can be varied by adjusting operation conditions. Therefore, we first investigate how the three parameters affect the rank of $\mathbf{E}(t)$ vs. time plots.

Figures 2a–c show the rank of $\mathbf{E}(t)$ vs. time plots with ω, β, and ε as the varying parameters, respectively. First, as ex-

Table 3. Predicted Mixing Times for Double-Port Feedings at Six Feeding Conditions for Airlift Reactors ($\alpha = 5$, $\beta = 0$, $\omega = 1$), Bubble Column Reactors ($\alpha = 5$, $\beta = 5$, $\omega = 1$), and Net Column Reactors ($\alpha = 5$, $\beta = 0.9$, $\omega = 1$); $\varepsilon = \pm 5\%$**

Feeding Condition	Parcel Number (Feeding Location)		Airlift Reactor			Bubble Column Reactor			Net Column Reactor		
	I	II	Amount of Feed at I	Amount of Feed at II	Predicted Mixing Time	Amount of Feed at I	Amount of Feed at II	Predicted Mixing Time	Amount of Feed at I	Amount of Feed at II	Predicted Mixing Time
(1)	2	25	14.00	14.00	8.4	14.00	14.00	8.2	14.00	14.00	5.4
(2)	5	22	14.00	14.00	11.7	14.00	14.00	4.3	14.00	14.00	4.7
(3)	6	22	(287.42)**	(−260.16)**	57.6	13.51	14.49	5	11.11	16.89	3.1
(4)	14	16	14.00	14.00	8.7	14.00	14.00	8.4	14.00	14.00	5.3
(5)	1	20	19.60	8.40	25.7	9.21	18.79	4.6	11.15	16.85	4.0
(6)	11	17	14.00	14.00	8.7	14.00	14.00	7.1	14.00	14.00	3.7

* Feeding conditions (1)–(3) give the shortest mixing times for airlift, bubble column, and net column reactors, respectively, whereas feeding conditions (4)–(6) give mixing times close to those achieved in conditions (1)–(3), but with feeding locations being more conveniently arranged for experiments.
**Unrealistic simulation results.

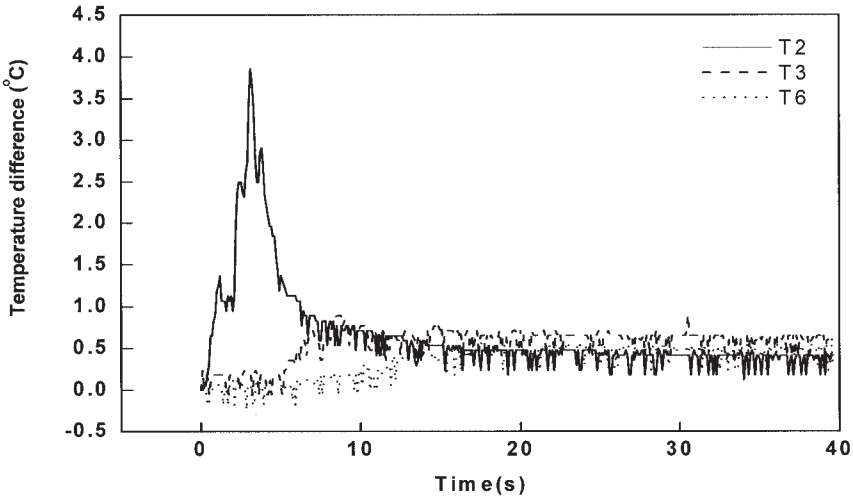

(a)

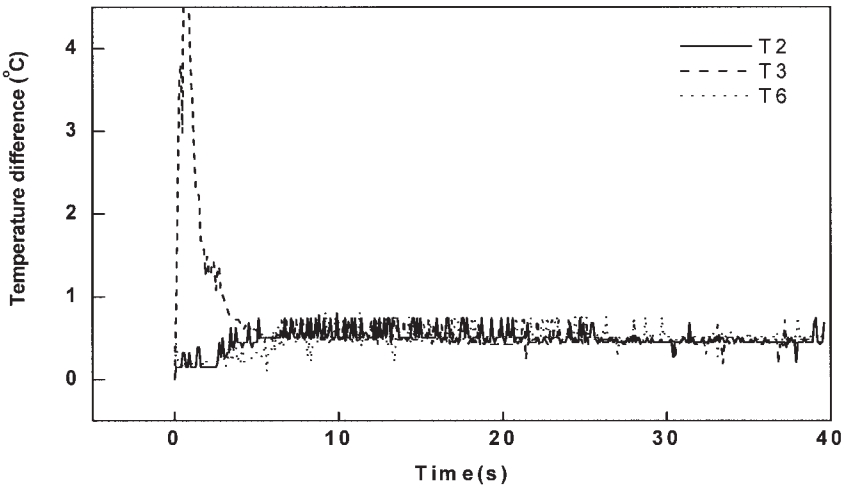

(b)

Figure 3. Temperature dynamics for (a) top feeding at parcel 2, and (b) side feeding at parcel 13 for bubble column reactors.

Comparison of (a) and (b) shows the dramatic effect of feedport location.

pected, the rank of $\mathbf{E}(t)$ reduces from the full rank of 28 at time zero to 1 at some longer times. If one demands the system to jump from one steady state to a new steady state in no time, the only way to achieve this is to divide the amount of feed into n equal portions and feed them from n feedports to the n well-stirred parcels. On the other hand, when the targeted mixing time is relaxed to a larger value, then even one single feedport can achieve the required mixing. Systems with a better mixing performance can achieve desired mixing at a targeted mixing time with fewer feedports. With the above, one concludes that systems with a better mixing performance have the curves located on the left side of the plot, whereas those with a poorer mixing performance have the curves located on the right side of the plot.

In Figure 2a, the effect of the parameter for main convective flow is examined. As expected, a faster main convective flow, a larger ω, leads to better mixing performance. Figure 2b reveals the superiority of net column reactors in mixing performance. This finding has been discussed in detail in Fu et al.[6] In Figure 2c, the effect of concentration tolerance is investigated. With a more relaxed tolerance, it is easier to achieve the desired mixing because the target concentration window is larger. Consequently, the more relaxed tolerance leads to fewer feedports required at a targeted mixing time.

Model predictions for optimal feeding locations and associated amounts of feed

In this subsection, we discuss model predictions for optimal feeding locations and associated amounts of feed for single-port and double-port feeding operations. Here, without loss of generality, we set the total amount of feed to be 28. For single-port feedings, the amount of feed is always 28 for the feedport. Table 2 lists some of the 28 solutions, corresponding to 28 feeding locations, for single-port feedings and the resulting mixing times predicted from Eq. 7 by using the preset

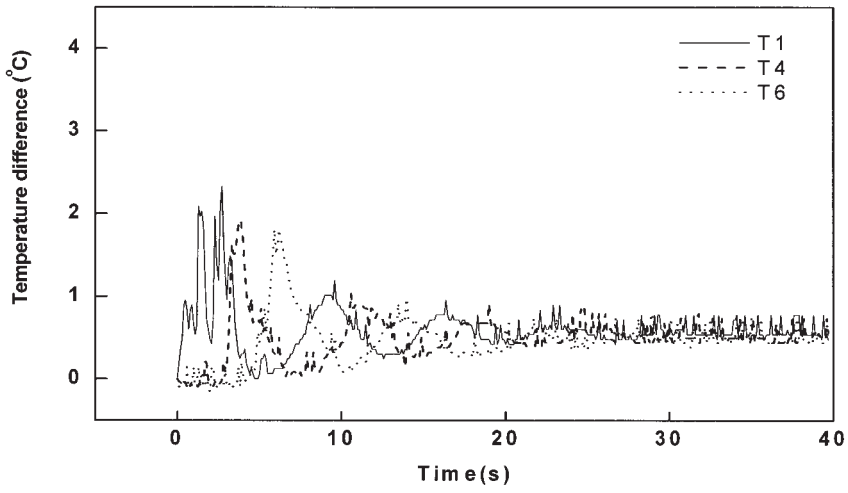

(a)

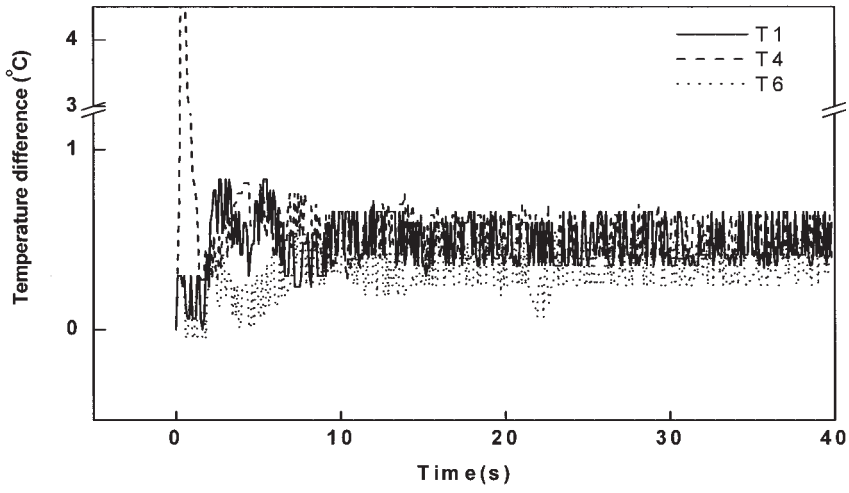

(b)

Figure 4. Temperature dynamics for (a) single-port top feeding at parcel 2, and (b) double-port feeding at parcels 14 (14) and 16 (14) for airlift reactors.

The advantage of double-port feeding practice in mixing is evident.

tolerance of ±5%. A few points can be observed from Table 2. First, airlift reactors show generally poor mixing ability regardless of feedport location. The influence of feedport location is overwhelmed by the strong circulatory flow pattern existing in airlift reactors. The feedport location, however, plays an important role in mixing performance for bubble column reactors. A suitable feedport location (such as parcel 13) can lead to mixing times even shorter than those of net column reactors. Net column reactors generally show good mixing ability with a moderate dependency on feedport location. Second, the common practice of top feeding (feeding from parcel 1 or 2) is shown not to be a good practice in terms of mixing performance. For single-port feeding in bubble column reactors, the best feedport location is at parcel 13, a middle side location. Once the tracer is fed into parcel 13, strong interactions between parcel 13 and parcel 14 will extract much of the tracer into parcel 14. The simulation results show that almost half of the feed gets transported into parcel 14. The half remaining in the downcoming stream continues to go down and the other half, transporting from parcel 13 to parcel 14, goes into the uprising stream.

As for double-port feedings, there are 378 possible combinations of feedport locations and thus 378 solutions for the initial condition vector. Table 3 lists six sets of feeding conditions, with conditions (1) to (3) representing the shortest mixing time cases for airlift, bubble column, and net column reactors, respectively, and conditions (4) to (6) the chosen feeding conditions for experimental verification for the three types of reactors, respectively. Feeding conditions (1) to (3), although giving the shortest mixing times for corresponding reactor type, are not convenient arrangements for experimental verification. Therefore, we pick the other three feeding conditions, (4)–(6), which have predicted mixing times close to those of conditions (1) to (3) and can be more conveniently carried out experimentally, for experimental verification. The experimental results are shown in the next section.

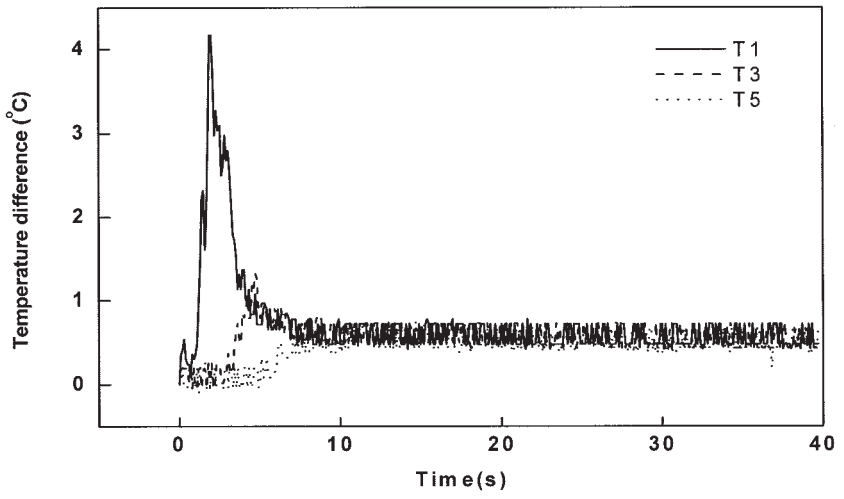

(a)

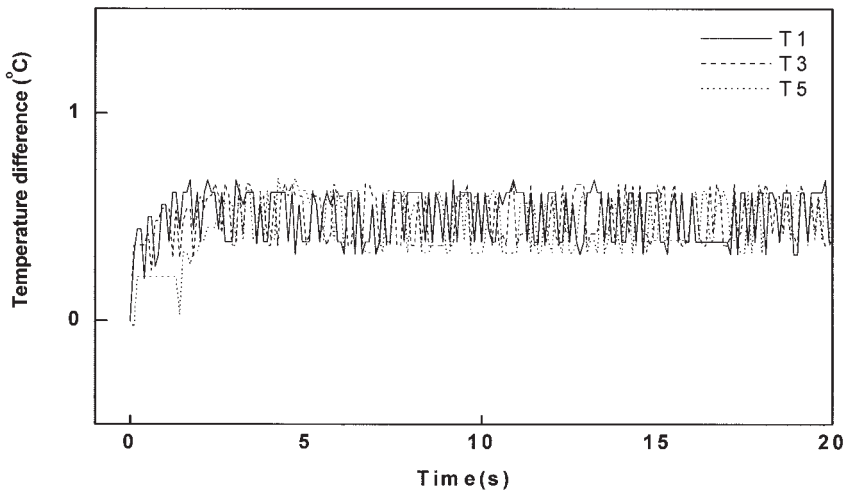

(b)

Figure 5. Temperature dynamics for (a) single-port top feeding at parcel 2, and (b) double-port feeding at parcels 11 (14) and 17 (14) for net column reactors.

The advantage of double-port feeding practice in mixing is evident.

There are a few things to note in Table 3. First, double-port feeding can dramatically reduce the mixing times, as evident from a comparison of Tables 2 and 3. This comes as no surprise because more feedports can more effectively homogenize the concentration disturbance. In practical applications, however, a greater number of feedports means more complications in design, operation, and maintenance. Second, it appears that net column reactors are still the most effective reactor type in terms of mixing performance among the three under the double feedport setting. Third, note that equal splitting of feed amount is not always the best practice, and the present devised scheme is able to suggest the optimal splitting of the total feed amount to different feedports.

Experimental verification for model predictions

Experiments are conducted to verify predictions of the proposed algorithm for single-port and double-port feeding operations. For single-port feedings, we have observed from Table 2 that feed port location can significantly affect the mixing performance of bubble column reactors. The side feeding practice at parcel 13 gives a much shorter mixing time than that achieved by the top feeding at parcel 2. In Figures 3a and b, we show the experimental results for temperature dynamics recorded at positions T2, T3, and T6 for top feeding at parcel 2 and side feeding at parcel 13, respectively. It is evident from the comparison of the two plots that the side feeding practice considerably shortens the mixing time compared to that of the top feeding practice. Similar results are obtained for airlift and net column reactors (data not shown). We show here only the most pronounced difference existing in bubble column reactors for illustration.

We have concluded from the comparison of Tables 2 and 3 that double-port feeding can give much better mixing performance than single-port feeding, particularly the common top

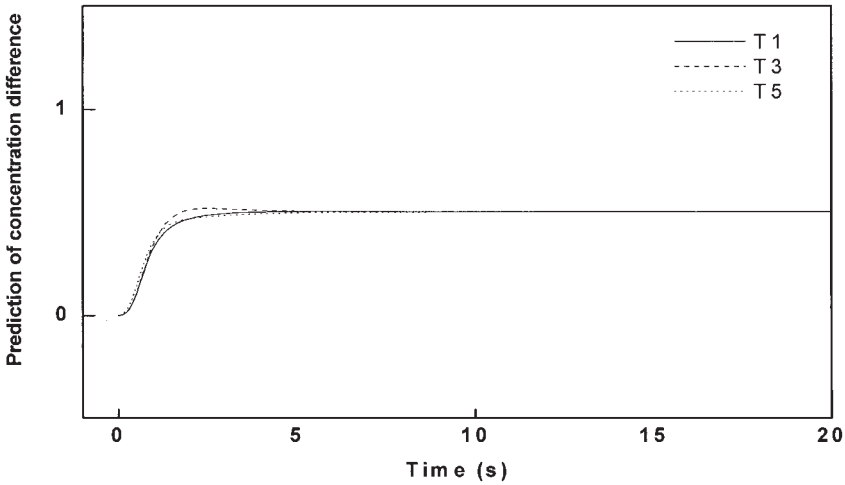

Figure 6. Temperature dynamics of the model predictions in the concentration dynamics for double-port feeding at parcels 11 (14) and 17 (14) for net column reactors, which agree quite well with the plot in Figure 5b.

feeding practice. In Figures 4 and 5, we illustrate this point by examining the experimental temperature dynamics for single-port and double-port feedings for airlift and net column reactors, respectively. To intensify the difference, we pick top feeding at parcel 2 for single-port feeding practice and feeding condition (4) for airlift reactors and condition (6) for net column reactors for double-port feeding practice as the comparison basis. Figures 4a and b are for temperature dynamics recorded at T1, T4, and T6 for single-port feeding at parcel 2 and double-port feeding at parcels 14 (14) and 16 (14), respectively for airlift reactors. Note here the numbers enclosed in parentheses represent the amount of feed at that feeding location. The temperature dynamics show the typical oscillatory pattern, coming from the strong circulatory flow pattern of airlift reactors. The improvement in mixing performance is apparent from the comparison of the two plots. The same conclusion can be drawn for net column reactors by comparing Figures 5a and b. In Figure 6, the corresponding model predictions for concentration dynamics at T1, T3, and T5 are presented to show the close agreement between experimental (Figure 5b) and predicted data (Figure 6). This also shows the appropriateness of using a thermal tracer to capture concentration dynamics in this system.

Feeding conditions (1) to (3) give the shortest predicted mixing times for airlift, bubble column, and net column reactors, respectively. Although the three feeding conditions give the shortest predicted mixing times for the three types of reactors, they are not convenient to be carried out experimentally. Therefore, we pick feeding conditions (4)–(6), which have the predicted mixing times close to those of conditions (1)–(3), for experimental verification. In Table 4, the predicted and experimentally determined mixing times for top feeding at parcel 2, side feeding at parcel 13, and double-port feedings under feeding conditions (4)–(6) in Table 3 are tabulated for comparison. Note that, to determine mixing times from experimental data, the temperature dynamics are first smoothed before comparison with a set tolerance range. Note also for model predictions the fitted values for ω are used instead of the set value of one as in Tables 2 and 3. As evident from Table 4, model predictions agree with experimental data quite well.

Conclusion

An algorithm based on solution of the inverse problem of a concentration dynamics is successfully developed to predict the optimal feeding practice in terms of mixing performance in tower-type reactors. The agreement between the model predictions and experimental results is excellent. The common top feeding practice is found ineffective in achieving efficient mixing in tower-type reactors because of the strong radial interactions that trap the feed species in the top region. On the other hand, double-port feeding can significantly improve the mixing performance for all three types of reactors. Furthermore, the superiority of net column reactors in mixing performance is demonstrated for both single-port and double-port feeding practices.

Table 4. Comparison of Predicted and Experimentally Determined Mixing Times Under an Air Flow Rate of 10 LPM*

	Mixing Time (s)					
	Predicted			Experimentally Determined		
Reactor Type	Top Feeding at Parcel 2	Side Feeding at Parcel 13	Double-Port Feeding	Top Feeding at Parcel 2	Side Feeding at Parcel 13	Double-Port Feeding
Airlift	15.9	16.7	5.5	16.8	16.9	5.7
Bubble column	21.2	6.8	3.3	23.0	7.2	3.5
Net column	13.5	8.4	3.2	14.3	9.0	3.4

*For double-port feeding, the feeding locations are: airlift reactors at 14 (14) and 16 (14), bubble column reactors at 1 (9.21) and 20 (18.79), and net column reactors at 11 (14) and 17 (14). The numbers in parentheses are the associated amount of feed.

Acknowledgments

The authors gratefully acknowledge the help of Yi-Ren Lin and Gia-Chi Chen of our department for carrying out some of the experimental work. Financial support from the National Science Council of the Republic of China under Grant 91-2214-E-007-014 (to S.-Y. Lu) is gratefully acknowledged.

Literature Cited

1. Deckwer WD. *Bubble Column Reactors*. New York, NY: Wiley; 1992.
2. Chisti MY. *Airlift Bioreactors*. New York, NY: Elsevier Applied Science; 1989.
3. Lee JM. *Biochemical Engineering*. Upper Saddle River, NJ: Prentice-Hall; 1992.
4. Fu CC, Wu WT, Lu SY. Performance of airlift bioreactors with net draft tube. *Enzyme Microb Technol.* 2003;33:332-342.
5. Wu WT, Wu JY. Airlift reactor with net draught tube. *J Ferment Bioeng*. 1990;70:359-361.
6. Fu CC, Lu SY, Hsu YJ, Chen CC Chen, Lin YR, Wu WT. Superior mixing performance for airlift reactor with a net draft tube. *Chem Eng Sci.* 2004;59:3021-3028.
7. Noble B, Daniel JW. *Applied Linear Algebra*. Upper Saddle River, NJ: Prentice-Hall; 1988.
8. Bequette BW. *Process Dynamics Modeling, Analysis, and Simulation*. Upper Saddle River, NJ: Prentice-Hall; 1998.
9. Joshi JB, Sharma MM. A circulation cell model for bubble columns. *Trans IChemE.* 1979;57:244-251.

Manuscript received Oct. 17, 2003, and revision received July 2, 2004.